Modifying the Electronic Orbitals of Nickelate Heterostructures via Structural Distortions

Hanghui Chen,[1,2,3] Divine P. Kumah,[3] Ankit S. Disa,[3] Frederick J. Walker,[3] Charles H. Ahn,[3,4] and Sohrab Ismail-Beigi[3]

[1]*Department of Physics, Columbia University, New York, New York 10027, USA*
[2]*Department of Applied Physics and Applied Mathematics, Columbia University, New York, New York 10027, USA*
[3]*Department of Applied Physics, Yale University, New Haven, Connecticut 06520, USA*
[4]*Department of Mechanical Engineering and Materials Science, Yale University, New Haven, Connecticut 06520, USA*

(Received 30 November 2012; revised manuscript received 15 February 2013; published 1 May 2013)

We describe a general materials design approach that produces large orbital energy splittings (orbital polarization) in nickelate heterostructures, creating a two-dimensional single-band electronic surface at the Fermi energy. The resulting electronic structure mimics that of the high temperature cuprate superconductors. The two key ingredients are (i) the construction of atomic-scale distortions about the Ni site via charge transfer and internal electric fields, and (ii) the use of three-component (tricomponent) superlattices to break inversion symmetry. We use *ab initio* calculations to implement the approach, with experimental verification of the critical structural motif that enables the design to succeed.

DOI: 10.1103/PhysRevLett.110.186402 PACS numbers: 71.10.−w, 73.20.−r, 73.21.Cd

A forefront area in condensed matter physics involves the modification of matter at the scale of individual atomic layers to form artificial systems whose properties differ significantly from their "parent" bulk forms. Transition metal oxides are paradigmatic: (i) their bulk forms display an array of physical phenomena, including magnetism, metal-insulator transitions, and superconductivity [1,2]; (ii) in principle, one can choose among various cations and their spatial ordering in the oxide lattice; and (iii) in practice, advanced layer-by-layer fabrication techniques can realize such heterostructures [3–5]. One current topic involves the engineering of electronic states in heterostructures in order to emulate the properties of high temperature copper oxide (cuprate) superconductors. A concrete proposal involves artificial heterostructuring of rare-earth nickelate materials, specifically atomically thin $LaNiO_3$ layers surrounded by insulating $LaAlO_3$ layers in the (001) direction, to fulfill four basic properties of carriers found in the cuprates and to realize a single-band two-dimensional (2D) Hubbard model: spin one-half, quasi-2D confinement, antiferromagnetic correlations, and lack of orbital degeneracy [6]. Figure 1(a) illustrates such a superlattice. This proposal has led to significant activity on nickelate heterostructures [7–18].

Experimentally, bulk $LaNiO_3$ is a metallic paramagnet with a single electron in doubly degenerate e_g bands [19,20]. *Ab initio* calculations confirm that two-component (bicomponent) $LaNiO_3/LaAlO_3$ heterostructuring reduces dimensionality by reducing the band dispersion of the out-of-plane $d_{3z^2-r^2}$ band compared to the in-plane $d_{x^2-y^2}$ band [7,9,13–16]. The reduced dimensionality also enhances the correlation effects and a Mott transition is observed [21], in line with other oxide systems where control over dimensionality and correlations can modify electronic band structure [22] or thermoelectric properties [23]. Ultrathin $LaNiO_3$ layers show a magnetic ground state in both experiment and theory [17,24]. However, orbital degeneracy is not much affected: pioneering experiments [13,15] and *ab initio* calculations [7,9,16] find that the population of the two e_g orbitals differ by ~5%–10%. Inclusion of Hubbard-type strong electronic correlations on Ni can produce a significant difference of orbital populations (i.e., orbital polarization) in a simplified effective low-energy description [7], but when both Ni and O orbitals are included in such a treatment, the orbital polarization is significantly reduced [14]. In contrast, cuprates have 100% orbital polarization which means that there are only $d_{x^2-y^2}$ bands at the Fermi level, while the $d_{3z^2-r^2}$ bands are lower in energy and completely filled due to strong crystal field splittings [25]. A key challenge is to modify bicomponent $LaNiO_3/LaAlO_3$ superlattices to achieve similarly large orbital polarizations.

In this Letter, we describe a materials design approach that engineers structural distortions in tricomponent superlattices to greatly enhance the orbital polarization. Figure 1 shows the design schematics. A first approach to overcoming the small orbital polarization in $LaNiO_3/LaAlO_3$ superlattices is to dope the $LaNiO_3$ layers: the $d_{3z^2-r^2}$ bands are narrow, so filling (or emptying) them may move the Fermi level into the $d_{x^2-y^2}$ bands. Replacing the $LaAlO_3$ layers by $LaTiO_3$, as displayed in Fig. 1(b), can achieve this goal: Ti^{3+} in $LaTiO_3$ has one electron in its d bands that seeks the lower energy Ni sites and dopes them n type. Below, we describe that while the doping is effective, it is insufficient to deliver full orbital polarization. An alternate approach stems from our and others' observations [18] that the surface Ni atoms on NiO_2-terminated $LaNiO_3$ thin films [see Fig. 1(c)] have the desired large orbital polarization due to eliminated bonds with the missing out-of-plane (apical) oxygen. However, using such a surface system in practice is challenging since the surface of a polar thin film can be subject

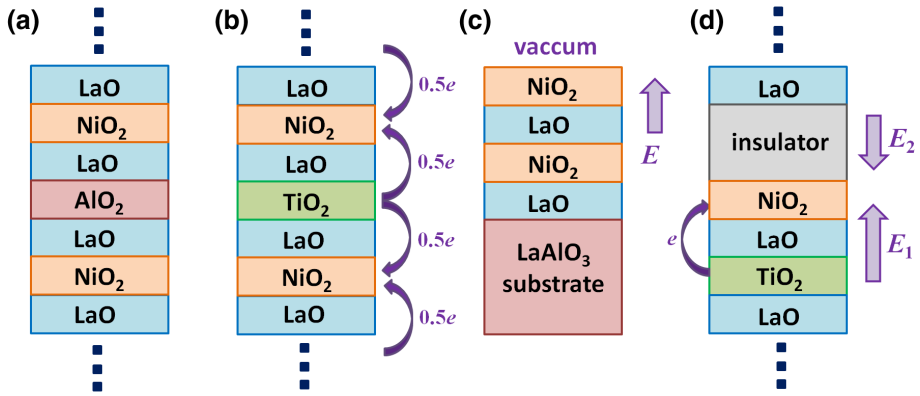

FIG. 1 (color online). Schematics of four nickelate heterostructures. (a) $(LaAlO_3)_1/(LaNiO_3)_1$ superlattice. (b) $(LaTiO_3)_1/(LaNiO_3)_1$ superlattice with nominal electron transfer from Ti to Ni. (c) NiO_2-terminated $LaNiO_3$ thin film on a $LaAlO_3$ substrate. (d) $(LaTiO_3)_1/(LaNiO_3)_1$/insulator superlattice with electron transfer and broken inversion symmetry. Arrows with "E" denote long-range electric fields in the material.

to various adsorbate perturbations that modify its properties (cf. Ref. [26]). Nevertheless, the main lesson of the thin film effect is to break or emulate the breaking of a Ni-O bond, and to realize this possibility in a three-dimensional superlattice we design structural distortions that greatly elongate the apical Ni-anion bonds sufficiently for orbital engineering purposes. We show that this approach is realizable with a tricomponent superlattice involving both the $LaTiO_3$ doping and an added wide-gap insulator: the Ti $\rightarrow$ Ni electron transfer, combined with the structural asymmetry and the requirement of a periodic potential in a superlattice, ensures the head-to-head electric field pattern depicted in Fig. 1(d). These fields move both apical anions away from the Ni and create a strong orbital polarization. In the remainder of this Letter, we use *ab initio* calculations to describe each step of the process and use experimental growth and characterization to verify the key structural properties that deliver the large orbital energy splitting. We point out that *ab initio* calculations have successfully described the large orbital polarization of high-temperature cuprate superconductors [27].

Our theoretical work employs density functional theory [28,29] within the supercell plane-wave pseudopotential approach [30], the QUANTUM-ESPRESSO package [31], the local density approximation [32,33], and ultrasoft pseudopotentials [34]. The superlattice direction and surface normal for thin films are along z. The structures are periodic in the x and y directions. In most of our calculations, the in-plane lattice vectors are fixed to the theoretical one of $LaAlO_3$ at $a = 3.71$ Å (2% smaller than experiment) in order to simulate a $LaAlO_3$ substrate for superlattice growth [35]. All remaining structural degrees of freedom are relaxed. We generate two e_g maximally localized Wannier functions [36,37] on each Ni using the WANNIER90 package [38]. By construction, these functions reproduce the *ab initio* antibonding conduction Ni e_g bands and provide onsite energies for the Ni e_g orbitals. Due to the well known underestimation of band gap in density functional theory, we use the rotationally invariant LDA + U approach [39,40], with an accepted literature value of $U_{\mathrm{Ti}} = 4$ eV on the Ti d states [41]. The main purpose of the U_{Ti} is not to describe correlated behavior on the Ti (since it will turn out to be a fully ionized donor), but simply to ameliorate the energy alignment between Ti and Ni d states. A detailed investigation shows a lack of dependence of the main physical properties on U_{Ti} [42]. We purposely have not included Hubbard U corrections on Ni in our theoretical calculations since LDA + U calculations for nickelates lead to mixed results. For bulk insulating rare-earth nickelates, $U_{\mathrm{Ni}} > 0$ is necessary to yield an insulating and magnetic, as opposed to a metallic and paramagnetic, ground state [43,44]. However, $U_{\mathrm{Ni}} > 0$ for bulk $LaNiO_3$ worsens agreement with experiment [45] (e.g., it predicts a magnetic ground state, contrary to its paramagnetic nature [16,44,45]). Important future directions involve seeing how our predictions may be modified by $U_{\mathrm{Ni}} > 0$, for example by magnetic behavior on Ni, and, more importantly, finding better ways of describing electronic correlations on the Ni site. Experimentally, we grow four unit cell thick films of $LaNiO_3$ on $LaAlO_3$ (001) substrates using molecular beam epitaxy, with the structure determined by synchrotron x-ray diffraction (see the Supplemental Material [46]). The diffraction is analyzed using the coherent Bragg rod analysis method [47] to produce electron density maps. The atomic position for each lattice site is identified by the centroid of the electron density near each site in the perovskite lattice. Further technical details on both theory and experiment are found in Ref. [46].

We begin with bulk $LaNiO_3$ strained to the $LaAlO_3$ substrate, which makes the $LaNiO_3$ weakly tetragonal ($c/a = 1.01$), since the strain mismatch is small. Unstrained bulk $LaNiO_3$ has space group $R\bar{3}c$. Table I shows a small difference between in-plane and out-of-plane Ni-O bond lengths. Figure 2(a) shows the e_g-projected electronic density of states (DOS); the two e_g DOS are similar, signaling negligible orbital splitting. The Wannier functions quantify this difference: Table I

TABLE I. Onsite energy differences Δ (second column), and Ni-anion bond lengths l (third and fourth columns) for the structures studied. The energy difference $\Delta = E(d_{x^2-y^2}) - E(d_{3z^2-r^2})$ is between the two Ni e_g maximally localized Wannier functions that describe the antibonding conduction bands. For the tricomponent superlattice (last row), the out-of-plane bonds are Ni-O and Ni-F in that order.

System	Δ (eV)	In-plane l (Å)	Out-of-plane l (Å)
Tetragonal $LaNiO_3$	0.07	1.86	1.88
$(LaAlO_3)_1/(LaNiO_3)_1$	0.08	1.86	1.86
$(LaTiO_3)_1/(LaNiO_3)_1$	0.23	1.86	2.00
NiO_2-terminated $LaNiO_3$ thin film	1.29	1.87	2.01
$(LaTiO_3)_1/(LaNiO_3)_1/(RbF)_2$	1.25	1.89	2.64/2.76

shows a 0.07 eV splitting of the onsite e_g energies, which is to be compared to the e_g bandwidth of ~4 eV.

Moving to the $LaNiO_3/LaAlO_3$ superlattice [see Fig. 3(a)], we find reduced out-of-plane hopping, as evidenced by the narrowed DOS of the $d_{3z^2-r^2}$ band [see Fig. 2(b)]. However, the Ni is bulklike, with uniform Ni-O bond lengths and nearly degenerate e_g orbitals (see Table I). There is a wider $d_{x^2-y^2}$ band and narrower $d_{3z^2-r^2}$ band, but the Fermi level cuts through the center of both bands, which is consistent with previous density functional theory calculations [7,9].

Next, we consider a $LaNiO_3/LaTiO_3$ superlattice [see Fig. 3(b)]. Bulk $LaTiO_3$ has space group $Pbnm$. Examination of the Ti d DOS [46] places them above the Fermi energy, thereby showing successful donation of the electron from Ti to Ni, as planned (see Ref. [42] for the effect of electron correlations on the electron transfer). However, the Ni DOS [see Fig. 2(c)] and the relatively small energy splitting (see Table I) show that although the $d_{3z^2-r^2}$ band is filled more than before, both e_g bands still contribute at the Fermi level. The doping is successful but insufficient to remove orbital degeneracy.

All of the above structures have inversion symmetry. A stoichiometric $LaNiO_3$ film breaks such symmetry with significant consequences. Figure 3(c) shows the structure of an epitaxial four unit cell NiO_2-terminated $LaNiO_3$ thin film on a $LaAlO_3$ substrate (modeled as a six unit cell slab of $LaAlO_3$). A polar distortion near the surface is clearly visible in Fig. 3(c) that is due to the polar nature of stoichiometric $LaNiO_3$ films along the (001) direction [48], with alternating $(LaO)^+$ and $(NiO_2)^-$ atomic planes, which creates a polar electric field pointing to the surface. As seen in Table I, this polar field causes a structural distortion that elongates the Ni-O bond of the surface Ni atom with the O below it. However, more important than the polarity is the fact that the surface Ni is missing an oxygen nearest neighbor and thus a Ni-O bond. Figure 2(d) shows a DOS with a narrow $d_{3z^2-r^2}$ band mostly below the Fermi energy and a $d_{x^2-y^2}$ band mostly above due to a large orbital energy splitting of 1.29 eV (see Table I). The reason for the large splitting is twofold. Foremost is that the formation of the surface has eliminated the apical Ni-O bond: the elimination of the Ni $d_{3z^2-r^2}$-O p_z hopping element lowers the $d_{3z^2-r^2}$ energy (since Ni e_g states are antibonding in nature). A secondary effect is the elongation of the Ni-O bond of the Ni with the O atom below: this elongation reduces the same hopping element and further lowers the $d_{3z^2-r^2}$ energy. This surface effect, whereby broken or elongated Ni-O bonds create a large orbital polarization, is the key that opens the door to the engineered tricomponent superlattices.

Because of the critical importance of this thin film structure to our approach, we have experimentally grown and characterized this system, as shown in Fig. 3(d). The $LaNiO_3$ film is NiO_2 terminated: the polar distortions (Ni-O z separations) in each NiO_2 layer compare well to the theory, and in both cases the polar distortions decay within a few unit cells of the surface. These data demonstrate that such thin film structures are physically realizable and have the atomic-scale structures that theory predicts.

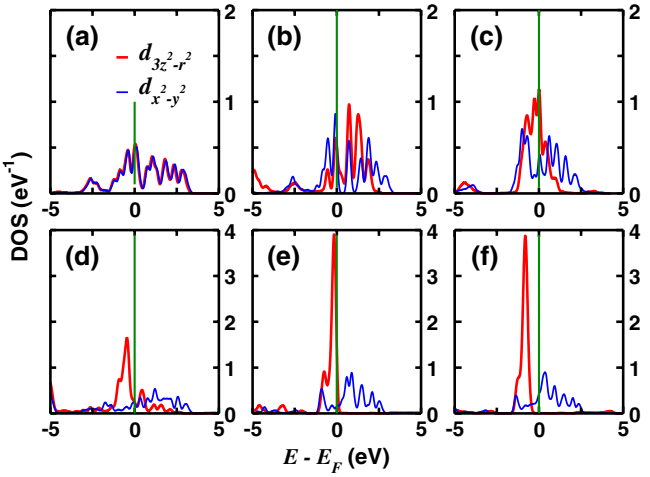

FIG. 2 (color online). Atomic projected densities of states (DOS): Ni $d_{3z^2-r^2}$ in red and Ni $d_{x^2-y^2}$ in blue. (a) Tetragonal $LaNiO_3$. (b) $(LaAlO_3)_1/(LaNiO_3)_1$ superlattice. (c) $(LaTiO_3)_1/(LaNiO_3)_1$ superlattice. (d) NiO_2-terminated $LaNiO_3$ thin film on a $LaAlO_3$ substrate (only surface Ni is shown). (e) $(LaTiO_3)_1/(LaNiO_3)_1/(RbF)_2$ superlattice. (f) Ba doped $(LaTiO_3)_1/(LaNiO_3)_1/(RbF)_2$ superlattice. Vertical solid green lines mark the Fermi level (set to zero energy).

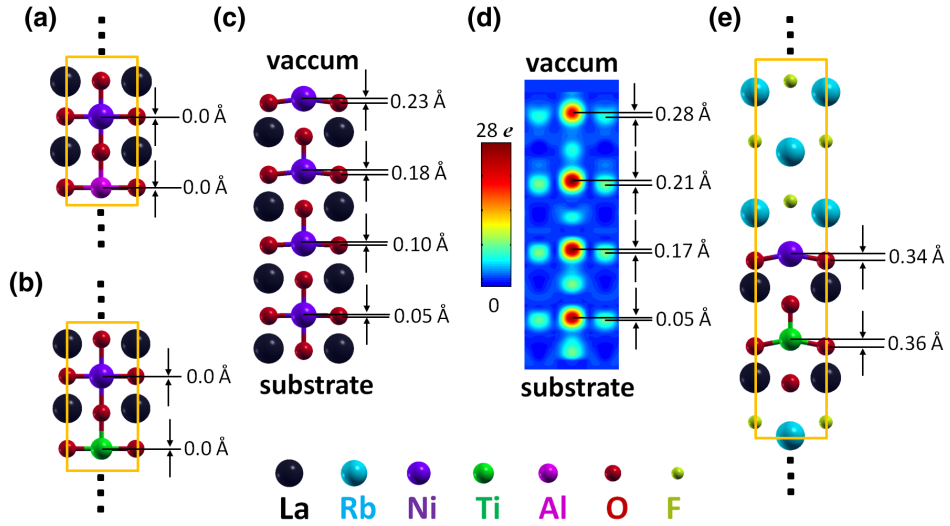

FIG. 3 (color online). Theoretically relaxed structures (a)–(c) and (e), as well as the experimentally determined thin-film structure (d) by synchrotron x-ray diffraction: (a) $(LaAlO_3)_1/(LaNiO_3)_1$ superlattice. (b) $(LaTiO_3)_1/(LaNiO_3)_1$ superlattice. (c) NiO_2-terminated four unit cell $LaNiO_3$ thin film on a $LaAlO_3$ substrate (substrate not shown). (d) Same as (c). The electron density map shown is a slice through the (101) plane of the $LaNiO_3$ thin film. (e) $(LaTiO_3)_1/(LaNiO_3)_1/(RbF)_2$ superlattice.

This comparison and benchmarking of the theory is important since we will be considering nonbulk structures and electronic configurations (e.g., Ni close to a formal +2 state and Ti close to a formal +4 state due to the electron transfer).

Based on all of this information, we now describe the tricomponent superlattices [see Fig. 1(d)], where we replace the vacuum in the thin film system by a wide-gap insulator. We have tested five candidates: $LaAlO_3$, $SrTiO_3$, BaO, RbF, and NaCl, which all have a good lattice match to $LaAlO_3$. All five show the same qualitative behavior described below. We focus on RbF, which has a very large gap [49]. Figure 3(e) shows a relaxed $(LaTiO_3)_1/(LaNiO_3)_1/(RbF)_2$ superlattice. The structure shows significant polar displacements, indicating internal electric fields. The displacements are consistent with the electric field pattern in Fig. 1(d), since the $LaTiO_3$ and $LaNiO_3$ layers have the La, Ti, and Ni displaced above the O (upwards electric field), while in the RbF the Rb atoms are displaced below the F atoms. The alternating direction of the electric field is due to the doping effect combined with the periodicity of the superlattice geometry: the Ti → Ni electron transfer creates a net field pointing from the $LaTiO_3$ to $LaNiO_3$ regions, and the periodicity requires an opposite field in the insulator. The bond lengths of the Ni with its neighboring anions show a large asymmetry between in-plane and out-of-plane directions, leading to a significant orbital splitting of 1.25 eV (see Table I). Figure 2(e) shows the DOS for this tricomponent superlattice: the narrow $d_{3z^2-r^2}$ band is essentially filled in the background of a wide $d_{x^2-y^2}$ band. Further electron doping can yield a single band system at the Fermi level with full orbital polarization. To accomplish that, we dope the RbF with Ba at an areal density of 0.25 Ba per Ni which requires a much larger in-plane unit cell (see Ref. [46] for details), with the resulting DOS shown in Fig. 2(f). The doping rigidly shifts the Fermi energy and fills the $d_{3z^2-r^2}$ band. The Fermi level now cuts only through a single band (the $d_{x^2-y^2}$ band) in direct analogy to cuprates.

We remark that while experimental realization of these tricomponent superlattices will be challenging due to the complexity of their structure, our approach is general and flexible, which permits the consideration of many possible materials combinations. For example, broken inversion symmetry occurs in the superconductors Li_2Pd_3B and Li_2Pt_3B where the lower symmetry causes Copper pairs to display interesting electronic properties [50].

In summary, we describe a general approach to realizing the single-band 2D Hubbard model on nickelate conducting planes. The key is to engineer the atomic-scale structure around the Ni to elongate some Ni-anion bonds compared to others. This approach creates a large e_g orbital energy splitting and orbital polarization, much like what is found in cuprate high-temperature superconductors. The two main tools are broadly applicable and robust: (i) charge transfer via doping (resulting in electric fields and polar displacements), and (ii) use of a tricomponent superlattice to break inversion symmetry. Given the generality of the approach, it can be applied to other systems to similarly engineer orbital polarizations.

Work at Yale is supported by Grant No. W911NF-10-1-0206 from the Army Research Office, with funding from the DARPA OLE Program, and NSF DMR 1119826 (CRISP). Computational facilities are supported by NSF Grant No. CNS 08-21132 and by the facilities and staff of the Yale University Faculty of Arts and Sciences High Performance Computing Center. Additional computations are carried out via the NSF TeraGrid and XSEDE resources

through Grant No. TG-MCA08X007. Use of the Advanced Photon Source was supported by the U. S. Department of Energy, Office of Science, Office of Basic Energy Sciences, under Contract No. DE-AC02-06CH11357.

[1] T. Wolfram and S. Ellialtioglu, *Electronic and Optical Properties of d-Band Perovskites* (Cambridge University Press, Cambridge, England, 2006).
[2] P. Zubko, S. Gariglio, M. Gabay, P. Ghosez, and J.-M. Triscone, Annu. Rev. Condens. Matter Phys. **2**, 141 (2011).
[3] C. H. Ahn, A. Bhattacharya, M. Di Ventra, J. N. Eckstein, C. D. Frisbie, M. E. Gershenson, A. M. Goldman, I. H. Inoue, J. Mannhart, A. J. Millis *et al.*, Rev. Mod. Phys. **78**, 1185 (2006).
[4] J. Mannhart, D. Blank, H. Hwang, A. Millis, and J.-M. Triscone, MRS Bull. **33**, 1027 (2008).
[5] J. M. Rondinelli and N. A. Spaldin, Adv. Mater. **23**, 3363 (2011).
[6] J. Chaloupka and G. Khaliullin, Phys. Rev. Lett. **100**, 016404 (2008).
[7] P. Hansmann, X. Yang, A. Toschi, G. Khaliullin, O. K. Andersen, and K. Held, Phys. Rev. Lett. **103**, 016401 (2009).
[8] S. J. May, T. S. Santos, and A. Bhattacharya, Phys. Rev. B **79**, 115127 (2009).
[9] M. J. Han, C. A. Marianetti, and A. J. Millis, Phys. Rev. B **82**, 134408 (2010).
[10] J. Son, P. Moetakef, J. M. LeBeau, D. Ouellette, L. Balents, S. J. Allen, and S. Stemmer, Appl. Phys. Lett. **96**, 062114 (2010).
[11] R. Scherwitzl, S. Gariglio, M. Gabay, P. Zubko, M. Gibert, and J.-M. Triscone, Phys. Rev. Lett. **106**, 246403 (2011).
[12] J. Chakhalian, J. M. Rondinelli, J. Liu, B. A. Gray, M. Kareev, E. J. Moon, N. Prasai, J. L. Cohn, M. Varela, I. C. Tung *et al.*, Phys. Rev. Lett. **107**, 116805 (2011).
[13] E. Benckiser, M. W. Haverkort, S. Brck, E. Goering, S. Macke, A. Fra, X. Yang, O. K. Andersen, G. Cristiani, H.-U. Habermeier *et al.*, Nat. Mater. **10**, 189 (2011).
[14] M. J. Han, X. Wang, C. A. Marianetti, and A. J. Millis, Phys. Rev. Lett. **107**, 206804 (2011).
[15] J. W. Freeland, J. Liu, M. Kareev, B. Gray, J. W. Kim, P. Ryan, R. Pentcheva, and J. Chakhalian, Europhys. Lett. **96**, 57 004 (2011).
[16] A. Blanca-Romero and R. Pentcheva, Phys. Rev. B **84**, 195450 (2011).
[17] A. V. Boris, Y. Matiks, E. Benckiser, A. Frano, P. Popovich, V. Hinkov, P. Wochner, M. Castro-Colin, E. Detemple, V. K. Malik *et al.*, Science **332**, 937 (2011).
[18] M. J. Han and M. van Veenendaal, Phys. Rev. B **84**, 125137 (2011).
[19] K. Sreedhar, J. M. Honig, M. Darwin, M. McElfresh, P. M. Shand, J. Xu, B. C. Crooker, and J. Spalek, Phys. Rev. B **46**, 6382 (1992).
[20] R. Eguchi, A. Chainani, M. Taguchi, M. Matsunami, Y. Ishida, K. Horiba, Y. Senba, H. Ohashi, and S. Shin, Phys. Rev. B **79**, 115122 (2009).
[21] J. Liu, S. Okamoto, M. van Veenendaal, M. Kareev, B. Gray, P. Ryan, J. W. Freeland, and J. Chakhalian, Phys. Rev. B **83**, 161102 (2011).
[22] K. Yoshimatsu, K. Horiba, H. Kumigashira, T. Yoshida, A. Fujimori, and M. Oshima, Science **333**, 319 (2011).
[23] T. D. Sparks, A. Gurlo, and D. R. Clarke, J. Mater. Chem. **22**, 4631 (2012).
[24] M. J. Han and M. van Veenendaal, Phys. Rev. B **85**, 195102 (2012).
[25] R. J. Cava, J. Am. Ceram. Soc. **83**, 5 (2000).
[26] R. V. Wang, D. D. Fong, F. Jiang, M. J. Highland, P. H. Fuoss, C. Thompson, A. M. Kolpak, J. A. Eastman, S. K. Streiffer, A. M. Rappe *et al.*, Phys. Rev. Lett. **102**, 047601 (2009).
[27] W. E. Pickett, Rev. Mod. Phys. **61**, 433 (1989).
[28] P. Hohenberg and W. Kohn, Phys. Rev. **136**, B864 (1964).
[29] W. Kohn and L. J. Sham, Phys. Rev. **140**, A1133 (1965).
[30] M. C. Payne, M. P. Teter, D. C. Allan, T. A. Arias, and J. D. Joannopoulos, Rev. Mod. Phys. **64**, 1045 (1992).
[31] http://www.quantum-espresso.org/.
[32] D. M. Ceperley and B. J. Alder, Phys. Rev. Lett. **45**, 566 (1980).
[33] J. P. Perdew and A. Zunger, Phys. Rev. B **23**, 5048 (1981).
[34] D. Vanderbilt, Phys. Rev. B **41**, 7892 (1990).
[35] Our key results do not rely on strain engineering and are expected to be robust versus epitaxial strain.
[36] N. Marzari and D. Vanderbilt, Phys. Rev. B **56**, 12 847 (1997).
[37] I. Souza, N. Marzari, and D. Vanderbilt, Phys. Rev. B **65**, 035109 (2001).
[38] http://www.wannier.org.
[39] A. I. Liechtenstein, V. I. Anisimov, and J. Zaanen, Phys. Rev. B **52**, R5467 (1995).
[40] S. L. Dudarev, G. A. Botton, S. Y. Savrasov, C. J. Humphreys, and A. P. Sutton, Phys. Rev. B **57**, 1505 (1998).
[41] T. Mizokawa and A. Fujimori, Phys. Rev. B **51**, 12 880 (1995).
[42] H. Chen, C. A. Marianetti, and A. J. Millis (to be published).
[43] S. Prosandeev, L. Bellaiche, and J. Iniguez, Phys. Rev. B **85**, 214431 (2012).
[44] H. Park, A. J. Millis, and C. A. Marianetti, Phys. Rev. Lett. **109**, 156402 (2012).
[45] G. Gou, I. Grinberg, A. M. Rappe, and J. M. Rondinelli, Phys. Rev. B **84**, 144101 (2011).
[46] See Supplemental Material at http://link.aps.org/supplemental/10.1103/PhysRevLett.110.186402 for further details on the calculations and thin film growth and characterization.
[47] Y. Yacoby, M. Sowwan, E. Stern, J. Cross, D. Brewe, R. Pindak, J. Pitney, E. M. Dufresne, and R. Clarke, Nat. Mater. **1**, 99 (2002).
[48] Bulk $LaNiO_3$ is metallic but has a finite screening length. Thus within a screening length of the polar (001) surface, one finds a non-negligible polar field which produces polar distortions of the ionic positions.
[49] Experimentally, we expect $LaAlO_3$ to be a logical starting choice for the insulator since the superlattice is then composed of the most structurally similar materials.
[50] H. Q. Yuan, D. F. Agterberg, N. Hayashi, P. Badica, D. Vandervelde, K. Togano, M. Sigrist, and M. B. Salamon, Phys. Rev. Lett. **97**, 017006 (2006).